APPLIED AND COMPUTATIONAL HARMONIC ANALYSIS 2, 350–362 (1995)

Radar Waveform Design and the Heisenberg Group

L. AUSLANDER

Department of Mathematics, City University of New York, 33 West 42nd Street, New York, New York 10036

F. GESHWIND

Department of Mathematics, Yale University, Box 208283 Yale Station, New Haven, Connecticut 06520

AND

F. WARNER

Department of Mathematics, City University of New York, 33 West 42nd Street, New York, New York 10036

Communicated by Ingrid Daubechies

Received April 5, 1994; revised February 6, 1995

This paper presents a number of constructions based on the Heisenberg group that are relevant to the problem of radar waveform design. All of the constructions are based on the modification of the Weil transform of a waveform. © 1995 Academic Press, Inc.

1. INTRODUCTION

It has been clear since the time of Woodward [21] that the goal of producing radar waveforms having prescribed ambiguity surfaces is not a realizable one. In his book, Woodward [21] states, "... the form of [the ambiguity function] cannot be arbitrarily chosen. The precise nature of the restrictions which must be placed on [ambiguity functions] have not been fully investigated." It is certainly the case that the last forty years have produced a vast literature dealing with the design of waveforms having specific ambiguity properties. The literature on the so-called "thumbtack" ambiguity surface, from Klauder [17] to Costas [11], provides one with a good case study on the nature of the work in this field up to now (see Blahut [9] or Cook and Bernfeld [10]). A great deal of progress has been made via special constructions, but no algorithm has been developed for synthesizing a waveform with an arbitrary ambiguity surface. One of the problems of course is that Woodward's above remark about the lack of knowledge concerning ambiguity functions still holds true, albeit not to the same extent. The set of all ambiguity functions, or "ambiguity space", is still a largely unexplored object (see Blahut [9] for more on ambiguity functions).

In this paper we propose new uses for certain Heisenberg group structures to aid in the exploration of ambiguity space. A good deal has been written on the applications of Heisenberg group theory to the theory of radar signal processing, but little of any practical engineering value has come of it. Throughout the theoretical development, the Weil transform has played a central role. Our goal is to reveal the modification of the Weil transform of a waveform as a tool for investigation of ambiguity surfaces in a very general and practical sense. We will define a waveform modification procedure that will have many of the classical radar construction as special cases.

The paper begins with a presentation of the group-theoretic setting in which we work, and this leads into a study of the important properties of the Weil transform. We define a discrete data structure called the "winding number data" of the Weil transform of a waveform and discuss some of its properties. We also detail the actual computation of this data. The role played by this data is a fundamental one in all of our investigations.

Three motivating examples using the winding number data follow in the next section. The first two examples present ways of constructing new waveforms from given ones. In the first the effects in terms of ambiguity are positive but a price is paid in the form of increased bandwidth. The second of the two examples produces a new waveform having better time-bandwidth properties than the original, but with some possible deleterious effects on the ambiguity surface. However, these negative effects may not necessarily hurt one in some particular applications. The last example uses the construction of the previous example to build waveforms for a multiresolution analysis of radar returns. We construct an example of a signal which has components

1063-5203/95 $12.00

on different scales, enabling one to look at a radar scene on more than one scale with the use of only one signal. This allows one to greatly reduce the amount of computation done by restricting the region where fine-scale calculations are done based on a large-scale calculation already performed on the same return.

2. MATHEMATICAL PRELIMINARIES

2.1. Heisenberg Group Theory

The essential tool in measuring the efficacy of a waveform $s(t)$ for a particular radar task is the ambiguity function

$$A_s(\tau, f) = \langle s(t-\tau)e^{-2\pi i f t}, s(t)\rangle = \int_{-\infty}^{\infty} s(t-\tau)e^{-2\pi i f t}\overline{s(t)}\,dt \tag{1}$$

where $\overline{s(t)}$ is the complex conjugate of $s(t)$. Consider

$$S(\tau)(s(t)) = s(t-\tau) \quad \tau \in \mathbf{R} \tag{2}$$

and

$$M(f)(s(t)) = e^{-2\pi i f t}s(t) \quad f \in \mathbf{R}. \tag{3}$$

Then $\tau \to S(\tau)$ is a representation of the reals $\mathbf{R}$ by a group of unitary operators on the Hilbert space $L^2(\mathbf{R})$. Similarly, $f \to M(f)$ is a representation of $\mathbf{R}$ by a group of unitary operators on $L^2(\mathbf{R})$. Noticing that $M(f)S(\tau)M(-f)S(-\tau) = e^{-2\pi i f \tau}I$, where I is the identity operator, we find that the set of unitary operators $\{M(f)S(\tau)(e^{2\pi i z}I)\}$ is a group $\mathcal{N}$. We will call $\mathcal{N}$ the Heisenberg group, as an abstract group, and the above representation of $\mathcal{N}$ the Dirac representation $\mathcal{D}$. It is one of the major results of classical harmonic analysis that the Dirac representation is irreducible. This means that there is no proper closed subspace $V \subset L^2(\mathbf{R})$ such that $DV = V$ for all $D \in \mathcal{D}$. It is easily verified that $e^{2\pi i z}I$ is the center of $\mathcal{D}$. In representation theory the function defined for $n \in \mathcal{N}$ by

$$P(n) = \langle D(n)s, s\rangle \quad s \in L^2(\mathbf{R}) \tag{4}$$

is called the matrix coefficient of the Dirac representation determined by s. This shows that the ambiguity function of s is essentially the matrix coefficients of the Dirac representation of $\mathcal{N}$ determined by s.

Now, consider the Heisenberg group $\mathcal{N}$ realized as $\{(x, y, z) | x, y, z \in \mathbf{R}\}$ with multiplication defined by

$$(x_1, y_1, z_1)(x_2, y_2, z_2) = (x_1 + x_2, y_1 + y_2, z_1 + z_2 + x_1 y_2), \tag{5}$$

together with its lattice subgroup defined by

$$\Gamma = \{(n_1, n_2, n_3) \in \mathcal{N} | n_1, n_2, n_3 \in \mathbf{Z}\}. \tag{6}$$

A function F invariant under the left action of the group Γ will naturally define a function on the coset space $\Gamma/\mathcal{N}$. The collection of all $F \in L^2(\Gamma/\mathcal{N})$ satisfying

$$F(x, y, z + u) = e^{2\pi i u}F(x, y, z) \tag{7}$$

forms a Hilbert space H_1. We note here one important property of the space H_1: any continuous function in H_1 must take on the value zero. The space H_1 may be used to define another representation of $\mathcal{N}$. Given $(n_1, n_2, n_3) \in \mathcal{N}$ and $F \in H_1$,

$$U(n)F = F((x, y, z)(n_1, n_2, n_3)) \tag{8}$$

defines $U(n)$ as a unitary operator from H_1 to H_1. This defines a representation of $\mathcal{N}$ on H_1 which is unitarily equivalent to the Dirac representation. The operator Θ providing the unitary equivalence is called the **Weil transform** (see [20]) and is defined by

$$\Theta(f)(x, y, z) = e^{2\pi i z}\sum_{a \in \mathbf{Z}} f(x + a)e^{2\pi i a y} \tag{9}$$

for f a Schwartz function on $\mathbf{R}$ and $(x, y, z) \in \mathcal{N}$. This operator extends to a unitary operator from $L^2(\mathbf{R})$ to H_1 which acts as an intertwining operator between our two representations of $\mathcal{N}$.

For the purpose of radar computations we may consider the z variable in the definition of $\Theta(f)$ to be equal to zero and deal with $\Theta(f)$ as a function of two variables. The following properties are immediate from the definition:

$$\Theta(f)(x, y + 1) = \Theta(f)(x, y) \tag{10}$$

$$\Theta(f)(x + 1, y) = e^{-2\pi i y}\Theta(f)(x, y). \tag{11}$$

Thus, $\Theta(f)$ is nearly a doubly-periodic function and it is determined by its values on the unit square. Note that the operator Θ is essentially the same as *Zak* or the *Weil-Brezin* transform common in the literature (see Folland [14]).

For more details of the mathematics, we refer the reader to Folland [14] or Miller [18].

2.2. The Weil Transform and Radar Waveforms

Pulse trains, signals consisting of a sequence of nonoverlapping copies of a fundamental signal or pulse, were introduced as an attempt to achieve the goal of a thumbtack-like ambiguity surface. Such signals were generalized to those having the form

$$s(t) = \sum_{l=0}^{N-1} p(t - lT)e^{-2\pi j\Omega_l t} \tag{12}$$

where $\Omega_l = \theta_l/T$ and $\{\theta_0, \ldots, \theta_{N-1}\}$ is a permutation of $\{1, \ldots, N\}$, T is the pulse repetition rate, and the support of $p(t)$ has length less than T. The irregular pattern of frequencies introduced by the permutation, sometimes called the firing sequence, accounts for the thumbtack-like ambiguity surface of the pulse train. Particularly successful such permutations relying on combinatorial properties of arrays were introduced by Costas [11].

These pulse trains are all special cases of signals of the form

$$s(t) = \sum_m \sum_n A_{mn} g(t - n)e^{2\pi imt} \tag{13}$$

where

$$\sum_m \sum_n |A_{mn}|^2 < \infty. \tag{14}$$

The formation of such signals from a basic signal $g(t)$ has a natural interpretation in terms of the representation theory of the Heisenberg group. The Weil transform plays the central role in this interpretation. Consider $s(t) = \sum_m \sum_n A_{mn} g(t - n)e^{2\pi imt}$ and let $p(x, y)$ be the doubly-periodic function with Fourier expansion given by

$$p(x, y) = \sum_m \sum_n A_{mn} e^{2\pi i(mx + ny)}. \tag{15}$$

Then it is easy to show that $\Theta(s)$ and $\Theta(g)$ are related by the equation

$$\Theta(s) = p(x, y)\Theta(g). \tag{16}$$

The formation of pulse trains in "signal space" thus amounts to multiplication by doubly-periodic functions in "Weil space" or H_1. The significance of this for the problem of creating a particular ambiguity surface is that we may compute the ambiguity function of f directly from $\Theta(f)$ by correlating $\Theta(f)$ with itself over the Heisenberg group:

$$A_f(\tau, \nu) = \int_0^1 \int_0^1 \Theta(f)(x, y)\overline{\Theta(f)(x + \tau, y + \nu)}e^{-2\pi ix\nu}\, dxdy. \tag{17}$$

Thus, cancellation properties of a signal $s(t)$ which may make it ideal for range and Doppler resolution are reflected in $\Theta(s)$.

2.3. The Winding Number Data and Its Discretization

In this section we will associate to any waveform a data set derived from the information contained in the phase of the Weil transform of the function.

We begin with a general definition. Let F be a continuous function from $\mathbf{R}^2$ to $\mathbf{R}^2$ and let C be an isolated, simply connected component of $F^{-1}(\{0\})$. Let Γ be a simple closed curve which winds exactly once around C and zero times around any other component of $F^{-1}(\{0\})$. The curve $F(\Gamma)$ may be continuously deformed into a curve Γ_N defined by

$$\Gamma_N(t) = e^{2\pi iNt} \quad t \in [0, 1], \tag{18}$$

where N is a uniquely determined integer. The *winding number of F around C* is defined to be this value N. It merely measures the total change in the phase of F, modulo 2π, around the boundary of a small neighborhood of a component of $F^{-1}(\{0\})$.

Now we may define the *winding number data* for a given waveform $s(t)$. We consider the components of $\Theta(s)^{-1}(\{0\})$ and associate with each component of the winding number of $\Theta(s)$ about that component. The components together with these winding numbers constitutes the winding number data for s.

The computation of winding numbers for the Weil transform of a function may be restricted to the unit square by equations (10) and (11). When we are dealing with the Weil transform of a waveform in practice we are using discrete data and we must take some care in measuring the phase change of the function. We proceed in a direct and computationally simple manner. Consider the unit square, $[1, 0] \times [0, 1]$, and divide the square into and array of $M \times M$ equal size boxes. To each oriented edge of each box we associate either 0, 1, or -1 as follows. Let F be the Weil transform of f and let ν_1 and ν_2 be consecutive vertices of one edge of a box. We want to measure the change in phase of F along the edge connecting ν_1 and ν_2. If we let $F(\nu_j) = r_j e^{2\pi i\theta_j}$, for $j = 1, 2$, the change in phase modulo π is then $2\theta_2 - 2\theta_1 = \Delta_{2,1}$. The integer $N_{2,1}$ assigned to the edge is then given by

$$N_{2,1} = \begin{cases} 1 & \text{if } 1 \leqslant \Delta_{2,1} \leqslant 2 \\ 0 & \text{if } -1 < \Delta_{2,1} < 1 \\ -1 & \text{if } -2 \leqslant \Delta_{2,1} \leqslant -1 \end{cases} \tag{19}$$

After this computation is done, the winding number for a square in the grid with vertices ν_1, ν_2, ν_3, and ν_4 is given by $N_{2,1} + N_{3,2} + N_{4,3} + N_{1,4}$. Thus, given a Weil transform $\Theta(f)$ that is sampled at a sufficiently high rate, and given an integer M' dividing M (M is the smallest scale of computation), the winding number data is an $M' \times M'$ matrix of integers whose nonzero elements correspond roughly to the zeros of $\Theta(f)$. These zeros play a role in attempting to

perform a windowed Fourier analysis using the function f as discussed in Section 3.1.1.

3. EXAMPLES OF WAVEFORM MODIFICATION

In this section we present a few examples of how the Weil transform may be used to construct or modify waveforms. In each case the zeros of the Weil transform will play an important role.

3.1. Approximate Orthonormal Bases

3.1.1. Ambiguity Functions and the Windowed Fourier Transform. The windowed Fourier transform arises naturally in the calculation of ambiguity functions. If we restrict out attention to integer lattice points (m, n), we see that $A_f(m, n)$ is given by

$$\int_{-\infty}^{\infty} f(t-m)e^{-2\pi int}\overline{f(t)}\,dt, \tag{20}$$

which is just a windowed Fourier coefficient of f with respect to the windowing function f. It is clear that the family of functions

$$\{f_{m,n} = f(t-m)e^{2\pi int} | m, n \in \mathbf{Z}\} \tag{21}$$

will be an orthonormal basis for $\mathbf{L}^2(\mathbf{R})$ if and only if the ambiguity function A_f is zero on the integer lattice away from the origin. One can easily show that this condition holds if and only if $|\Theta(f)| = 1$ almost everywhere.

There are some immediate problems in trying to take advantage of the above characterization of windowed bases. In general, one would like to compute with waveforms that have good smoothness properties as well as having

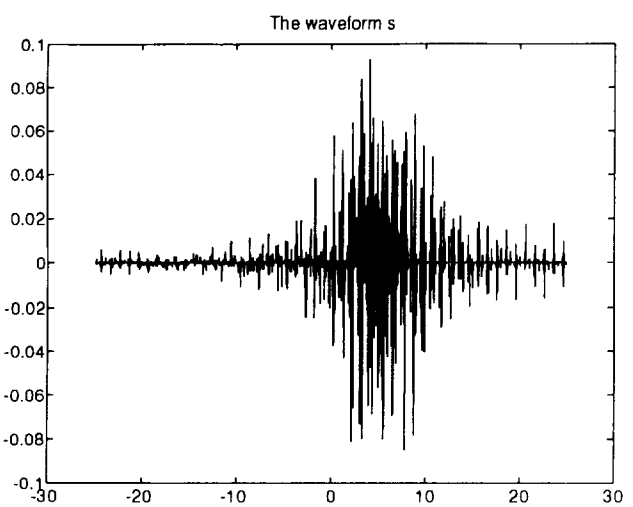

FIGURE 1

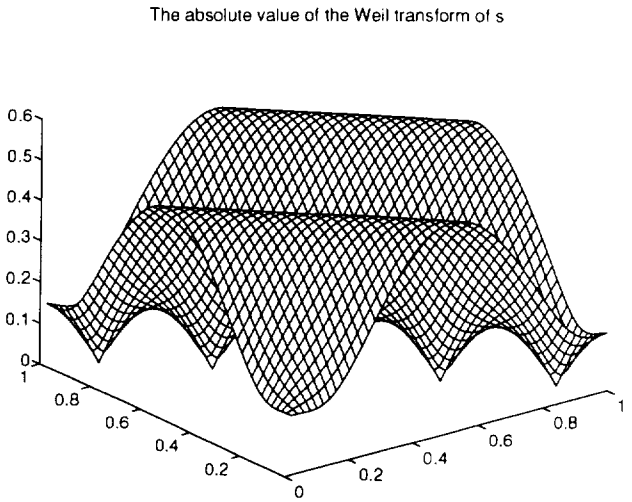

FIGURE 2

fast decay at infinity. In this case, Balian's Theorem (see Daubechies [12]) implies that the collection of functions $\{f_{m,n}\}$ defined above will not be a basis (in fact, it will not even be a frame). We must also deal with the fact that $\Theta(f)$ will be a function in H_1, and if it is even continuous, it must have a zero and will not satisfy the condition $|\Theta(f)| = 1$ almost everywhere.

One way around some of these difficulties is to approximate in the following way: given a waveform f, replace $\Theta(f)$ by $\Theta'(f)$ defined as

$$\Theta'(f) = \frac{\Theta(f)}{|\Theta(f)|} \tag{22}$$

and then approximate $\Theta'(f)$ by some nicer function in H_1. We refer to a sequence of functions $F_i \in H_1$ converging in $\mathbf{L}^2$ to $\Theta'(f)$ as an *approximate orthonormal basis.* See Auslander and Geshwind [2] and [3].

3.1.2. Example of Approximate Orthonormal Basis Calculation. For a given waveform s, one method of achieving the approximation described in the last section is simply to force the absolute value of the $\Theta(s)$ towards one away from the zeros of $\Theta(s)$. We begin our example with Fig. 1, which presents the waveform s that we will be working with. We will postpone a description of the construction of s until Section 3.2.

We will construct a new waveform by modifying $\Theta(s)$, whose absolute value is pictured in Fig. 2. In order to force the absolute value to be close to one we replace $|\Theta(s)|$ by some root of $|\Theta(s)|$, while keeping the phase of $\Theta(s)$ the same. For the example presented here, the limited dynamic range of the data allows us to produce a reasonable $\Theta'(s)$ using only the tenth root (in general, one might take a much

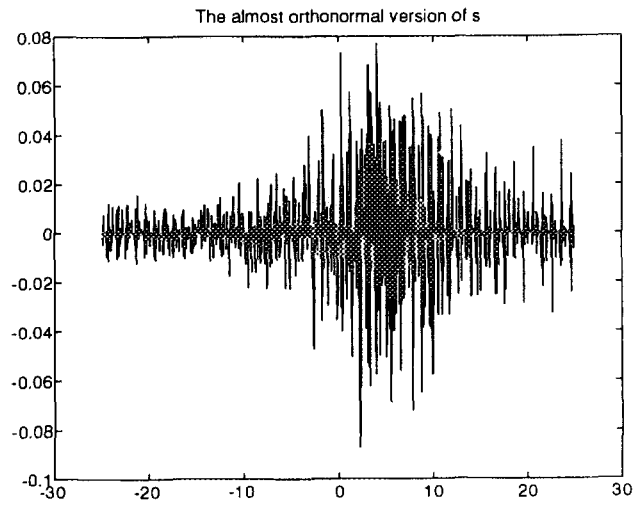

FIGURE 3

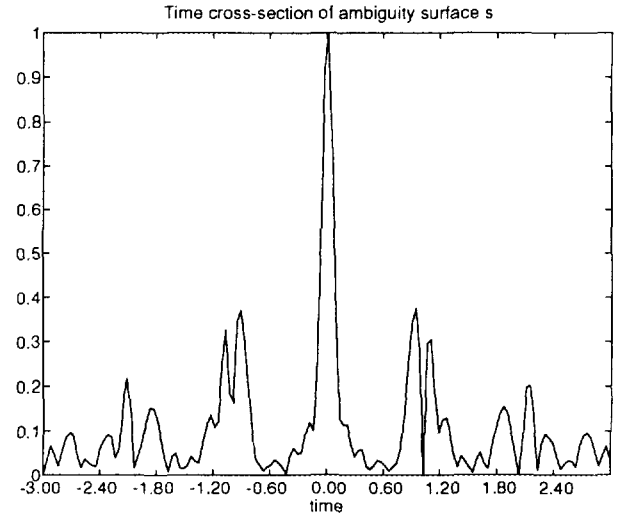

FIGURE 5

larger root). That is, if $\Theta(s)(x, y) = re^{i\theta}$ we replace r by the tenth root of r and we do not change θ. This produces a new H_1 function $\Theta'(s)$ and we produce our new waveform's by the applying the inverse Weil transform:

$$s' = \Theta^{-1}(\Theta'(s)). \tag{23}$$

The new waveform, the "almost orthonormals" in the figures, and its Weil transform are shown in Figs. 3 and 4. Computing the two ambiguity surfaces we see a very similar scene with some significant differences. Figures 5 and 6 show cross-sections of the two surfaces with the frequency variable set equal to zero. The surface for s' reveals precisely the effect of replacing s by s': the largest sidelobe at the first lattice point decreases in size from nearly .4 to just above .25, and the next second largest sidelobe decreases from slightly over .2 to a little more than .15. However, the violent modification of absolute value produces a significant increase in bandwidth.

3.2. *Prescribing Winding Number Data*

The waveforms s and s' of the previous section have by construction the same winding number data. Though that data was not explicitly used, it is clear from the example that the zeros and the phase around the zeros of $\Theta(s)$ are playing a significant role in determining the ambiguity properties of s. In this section we detail a method of

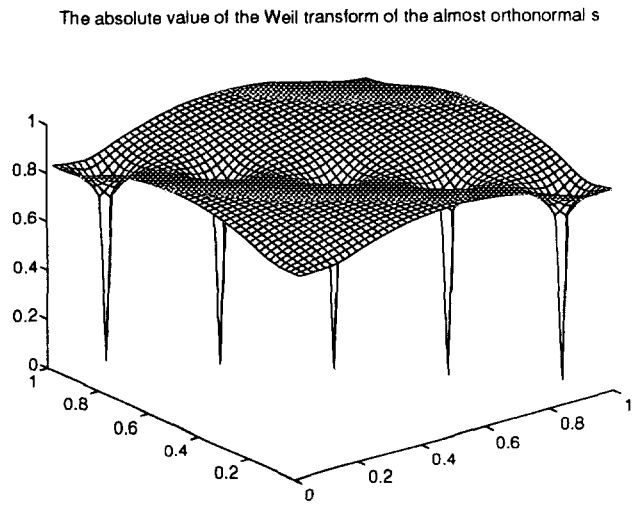

FIGURE 4

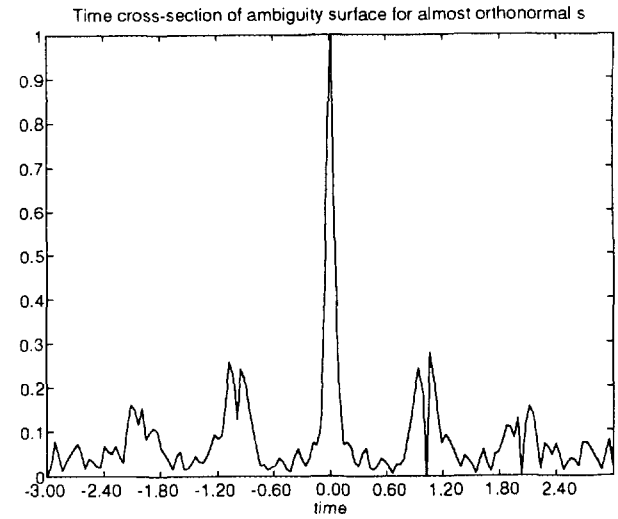

FIGURE 6

constructing waveforms having prescribed winding number data.

3.2.1. The Details of the Construction. Consider a waveform s together with its winding number data. The winding number data now will play a role of input for the construction of a new signal whose Weil transform has a similar winding number pattern. Let $g(t) = e^{-\pi t^2}$ and $\Theta(g) = G$. On the unit square, the function $G(x, y)$ is essentially equal to the product of $e^{-\pi x^2}$ and θ_3, the third classical Jacobi theta function. Hence, G has one zero in the unit square, at $(\frac{1}{2}, \frac{1}{2})$, with a winding number of one (see Auslander and Tolimieri [6]). Denote by $G_{\tau,\alpha}$ the Weil transform of g shifted in time and frequency so that its zero in the square is at (τ, α). Each such location (τ, α) can be thought of as a location in the winding number matrix in the obvious way. Given this identification, we define $G'_{\tau,\alpha}$ to be $G_{\tau,\alpha}$ if the winding number is 1 and $\overline{G_{\tau,\alpha}}$ if the winding number is -1. In general, if the winding number at location (τ, α) is $n, G'_{\tau,\alpha}$ is derived from $G_{\tau,\alpha}$ by keeping its modulus the same and multiplying its argument by n at every point in the unit square. We then form the following product

$$\prod_i G'_{\tau_i,\alpha_i}, \tag{24}$$

where the product is taken over all non-zero winding numbers in the winding number matrix. Our new waveform derived from the winding number data for s is denoted s' and is given by

$$s' = \Theta^{-1}\left(\prod_i G'_{\tau_i,\alpha_i}\right). \tag{25}$$

Now we may describe explicitly the waveform used in the example of the previous section. Its construction is just that given above for a specific choice of winding number matrix. We have chosen five zeros along the diagonal with winding numbers 1, 7, 10, -13, and -4. Nothing in the above construction says we must start with a waveform. It is just as reasonable to begin with a winding number matrix, provided the winding numbers are chosen to add to one. This choice of winding numbers gives us a function in H_1 and we obtain the waveform by applying Θ^{-1}.

Note that in general one must be careful when applying Θ^{-1} since not all functions on the square are in the image of Θ. However, if the winding number data of s is calculated correctly (or chosen judiciously), then we will necessarily have the correct number of complex conjugates in the product used to define s' and applying Θ^{-1} will be legitimate.

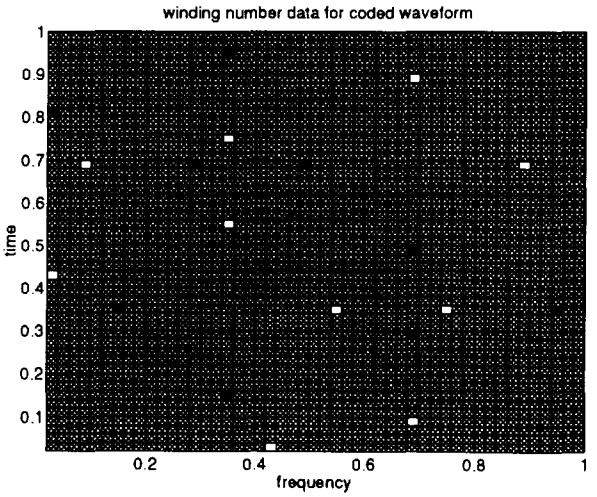

FIGURE 8

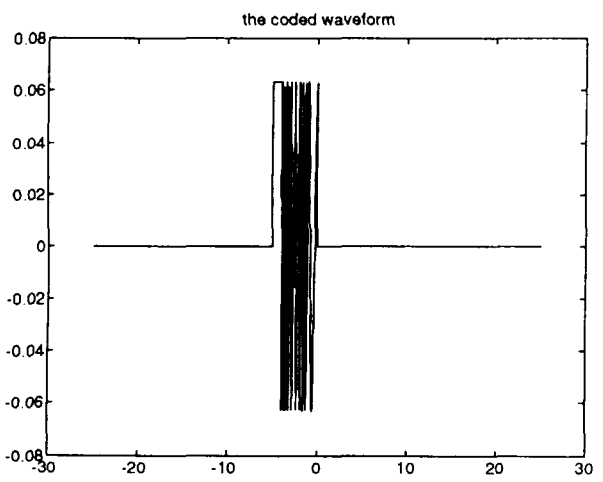

FIGURE 7

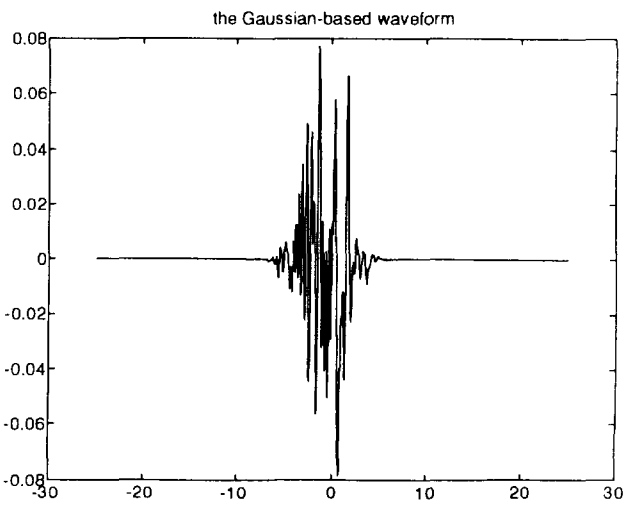

FIGURE 9

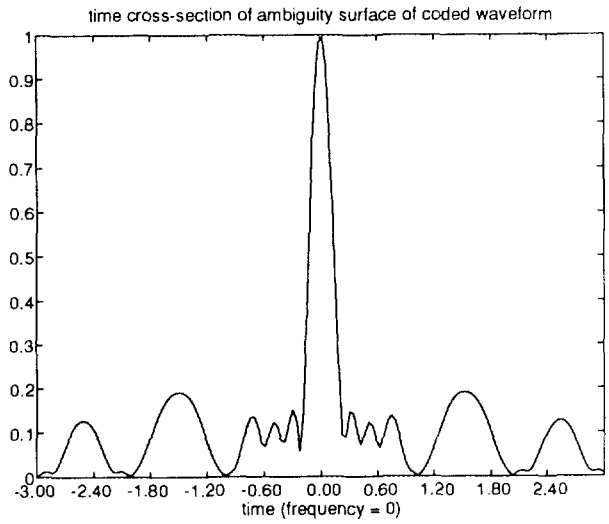

FIGURE 10

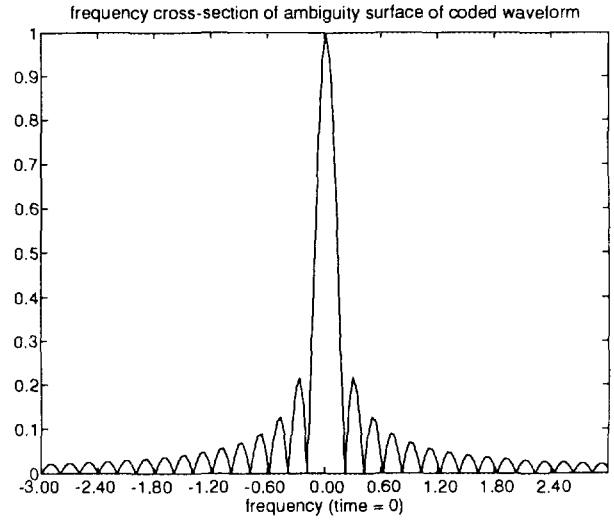

FIGURE 12

3.2.2. An Example. For our example we take a rectangular pulse and form a frequency-hopped pulse train $s(t)$ given by

$$s(t) = \sum_{j=1}^{n} \chi_{[0,1]}(t - j)e^{2\pi i\sigma(j)t} \tag{26}$$

having Weil transform is given by

$$\Theta(s)(x, y) = \sum_{j=1}^{n} e^{2\pi i(jx+\sigma(j)y)} \tag{27}$$

where σ is a permutation of $\{0, 1, \ldots, n-1\}$.

The permutation σ is given by (13240), and the signal, called the "coded waveform", and its winding number data are shown in Figs. 7 and 8. The white squares in the winding number picture correspond to 1s in the matrix and the black squares to $-1s$, with the gray representing 0. The constructed signal s', referred to as the "Gaussian-based waveform", is shown in Fig. 9.

A comparison of the ambiguity surfaces of the two waveforms reveals some interesting similarities and differences. For each of the ambiguity surfaces we consider four cross-sections: the time-axis section, the frequency axis section, and the two diagonal sections. These are shown in pairs by cross-section in Figs. 10–17, with the full surfaces shown for completeness in Figs. 18 and 19. It is reasonable to

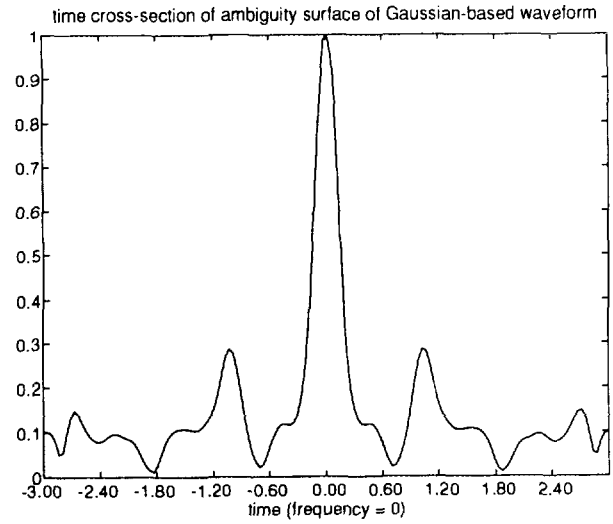

FIGURE 11

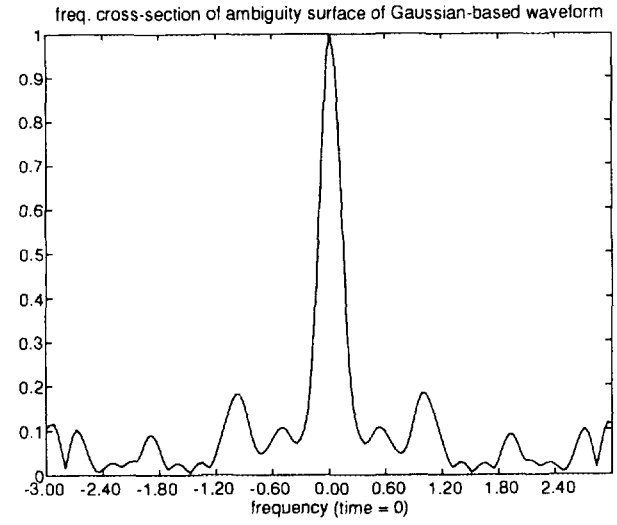

FIGURE 13

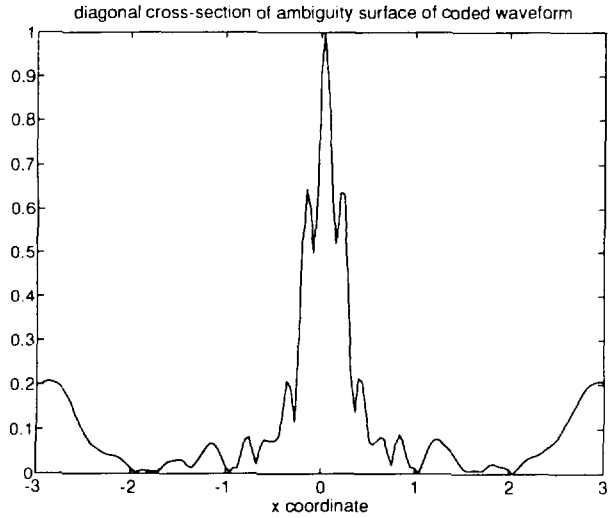

FIGURE 14

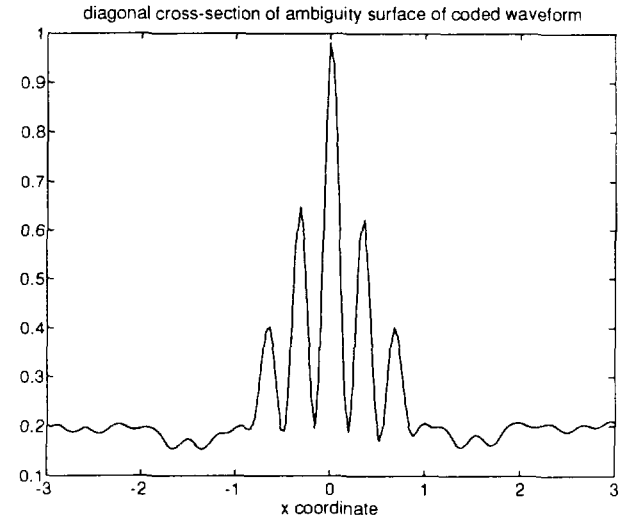

FIGURE 16

say that the cross-sections in each case are quite similar in that the size, if not the location, of the highest sidelobes differs by no more than .1. Of the two diagonal comparisons, the one with the very bad behavior in the Gaussian case is worth a particularly close look. In the case of the coded waveform, the surface levels off fairly close to the main lobe, revealing the cancellation present in the waveform that is absent from the Gaussian waveform. However, both sections show high sidelobes in a small neighborhood of the main lobe, and these could have been predicted by examining the winding number data in Fig. 8 (note the diagonal alignment of the zeros).

It is also of interest to consider one of the motivations for this construction. In the approximate orthonormal basis example, a big problem is the large increase in bandwidth caused by the modification. In this case, a comparison of the Fourier transforms of s and s', whose real parts are shown in Figs. 20 and 21, reveals something very different but not unexpected (see Auslander *et al.* [5]): the Fourier transform of s' is less oscillatory and (essentially) compactly supported, in contrast to that of s. Our building block of $\Theta(e^{-\pi t^2})$ was chosen with this in mind. In fact, one of the virtues of this construction is the production of waveforms with similar winding number data but with much better bandwidth properties.

3.3. Multiresolution Analysis of Radar Returns

The classical goal of radar is to determine the position and velocity of the target in question. We procede by send-

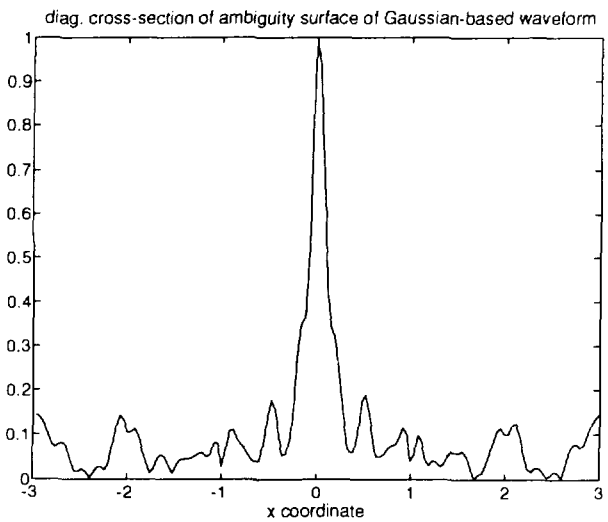

FIGURE 15

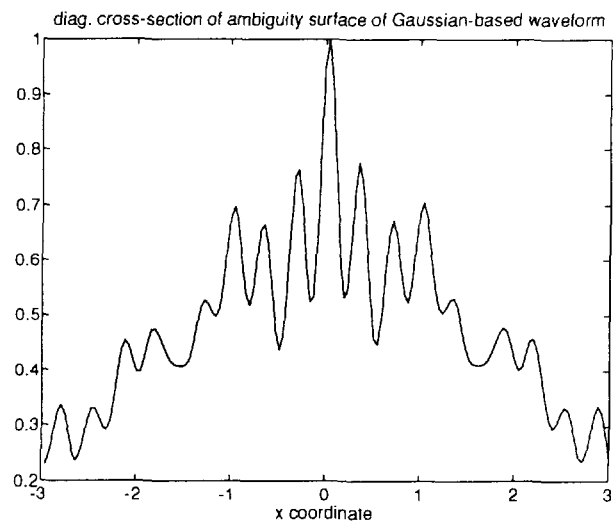

FIGURE 17

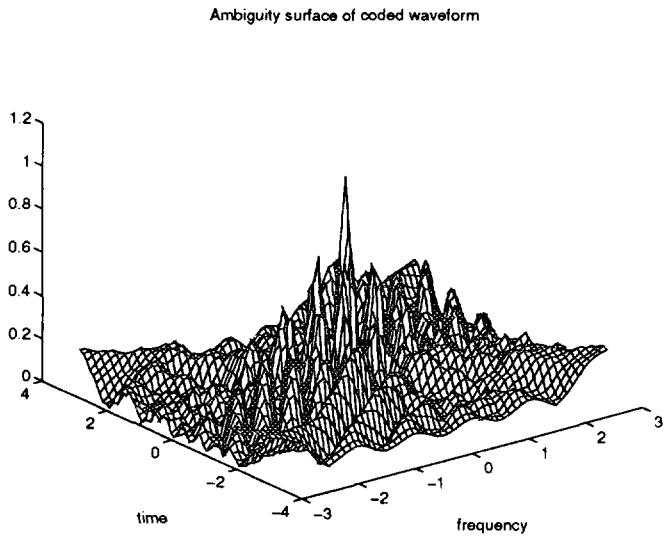

FIGURE 18

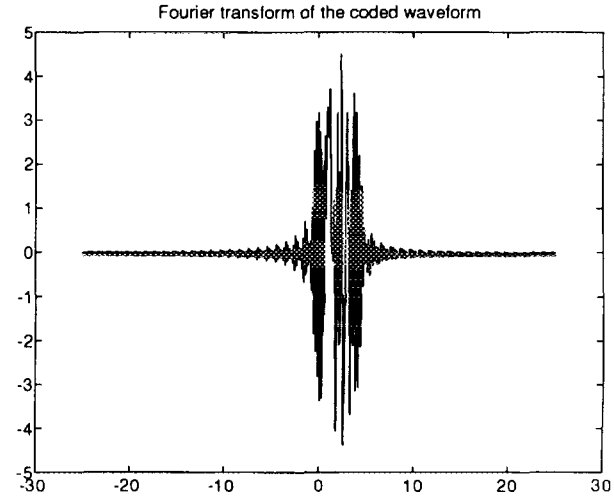

FIGURE 20

ing out a signal $s(t)$, and, under the narrow-band assumption, we receive a return of the form $r(t) = s(t + \tau)e^{2\pi i\theta t}$. Our task is to determine the range shift τ and the Doppler shift θ as accurately as possible in a *computationally efficient manner.*

3.3.1. The Multiresolution Idea. What we propose to do is to send out a signal $s(t)$ which is an orthogonal sum of signals $s_1(t)$ and $s_2(t)$. The processing of the return $r(t)$ then proceeds by first computing the cross-ambiguity surface of $s(t)$ and $r(t)$ at a particular scale, giving us bins where we believe the targets are located. We then restrict our attention to these particular binds, in which we compute the cross-ambiguity function of $r(t)$ and $s_2(t)$ on a much finer scale. The careful selection of the radar waveforms $s_1(t)$ and $s_2(t)$ will allow the determination of fine-scale structure present in the return $r(t)$, without having to compute at this resolution over the entire scene.

3.3.2. Particulars of the Construction. We begin with two functions S_1 and S_2 in Weil space (H_1) chosen so that:

1. The main lobe of the autoambiguity function of $\Theta^{-1}(S_2)$ is relatively narrow compared with that of $\Theta^{-1}(S_1)$.
2. S_1 and S_2 are orthogonal to one other.

In general, we may modify our initial choice of functions by "shaping" them with some doubly periodic function $p(x, y)$ with the property that $|p(x, y)| = 1$ everywhere. This pro-

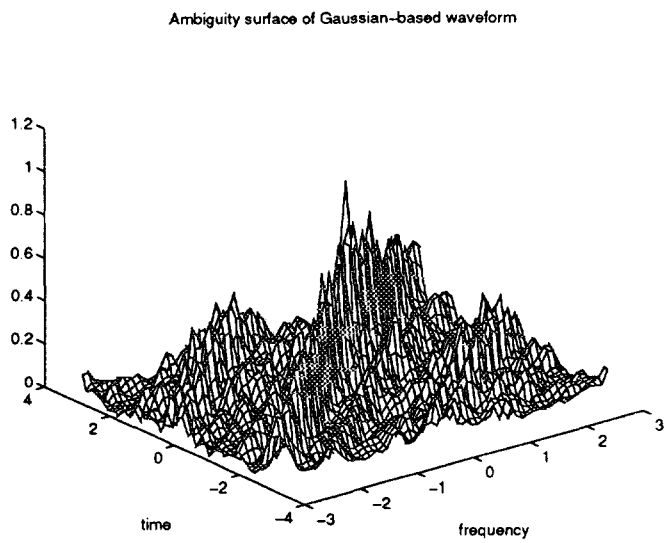

FIGURE 19

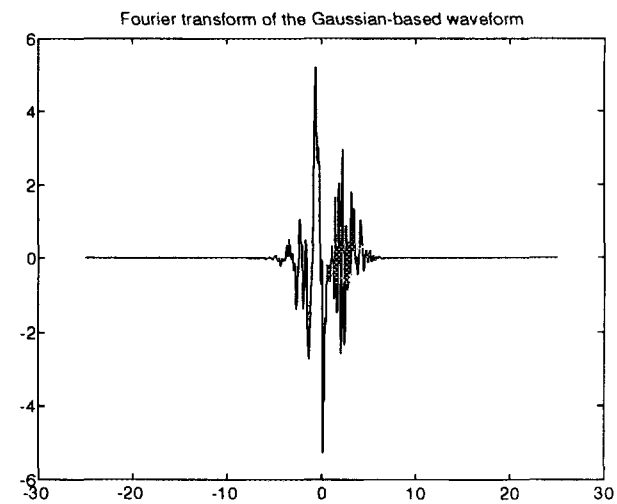

FIGURE 21

vides a way of modifying ambiguity surfaces without destroying orthogonality. However, "nice" shaping functions will have zeros and hence they will destroy orthogonality between the waveforms. This can be dealt with using the approximate orthonormal construction to preserve the zseros and phase of $p(x, y)$, which are the factors truly at work in doing the "shaping". Denote the resulting doubly periodic function by M. The two functions $s_1(t)$ and $s_2(t)$ are then given by:

$$s_1(t) = \Theta^{-1}(MS_1) \quad \text{and} \quad s_2(t) = \Theta^{-1}(MS_2). \tag{28}$$

Since M has absolute value one nearly everywhere and Θ^{-1} is unitary, $s_1(t)$ is nearly orthogonal to $s_2(t)$ and we let $s(t) = s_1(t) + s_2(t)$ be the signal we send out.

The basic procedure for multiresolution analysis of radar returns is now easy to state precisely. We send out the signal $s(t)$ as defined above, and we receive a return $r(t)$. We then compute the cross-ambiguity surface $|A_{s,r}|$ (defined exactly as A_s with r playing the role of the second occurrence of s in the integral) on a grid whose size is determined by the width of the main lobe of the ambiguity surface $|A_{s,s}|$. We select the bin or bins corresponding to high correlation, and we then compute $|A_{s_2,r}|$ inside these bins on a grid whose size comes from the main lobe of $|A_{s_2,s_2}|$ and which is finer than the original grid by construction. There are some immediate benefits to doing this:

1. The narrower peak of $|A_{s_2,s_2}|$ will serve to tell us where inside the larger bin the target actually lies, something that computing only with the fatter ambiguity surface would not do.

2. We only do the fine-scale calculation in a very limited region given to us by the coarse-scale calculation, thus saving valuable time in computing.

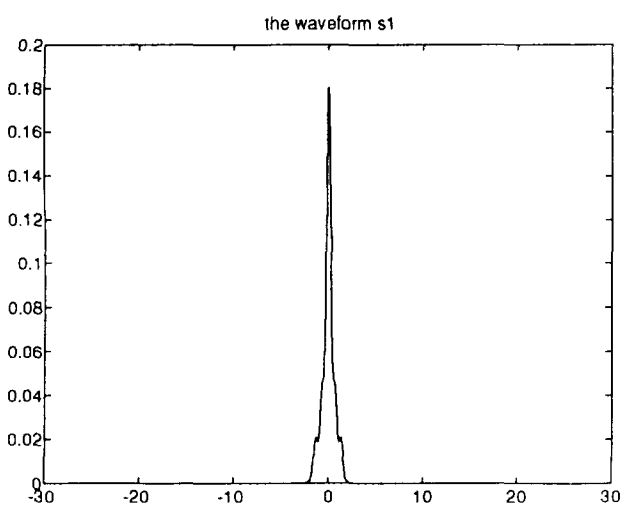

FIGURE 22

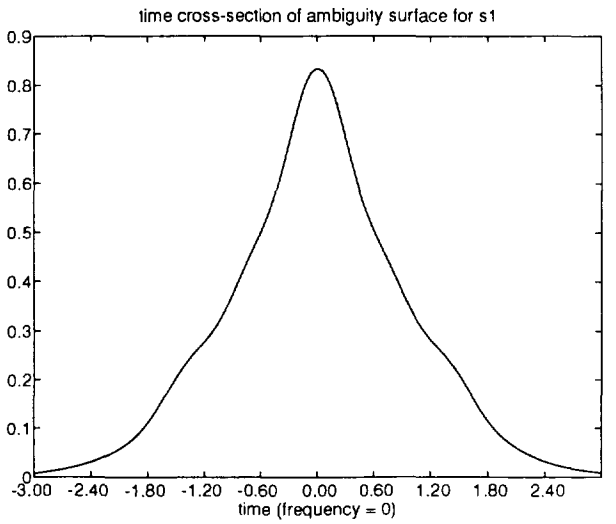

FIGURE 23

3. We obtain coarse-scale *and* fine-scale information using only one signal.

The key point in all of this is that the main lobe of $|A_{s_2,r}|$ should resemble that of $|A_{s_2,s_2}|$ due to orthogonality. This analysis can be extended to more than two levels of resolution—we need only start with a greater number of functions with the requisite orthogonality properties.

3.3.3. A Numerical Example. Here we present an example based on the previous section. We must construct waveforms s_1 and s_2 such that the ambiguity surface of s_1 has a very broad main lobe and that of s_2 a narrow main lobe, with s_1 orthogonal to s_2. Our choice of waveforms is motivated by the Gaussian product construction of section 3.2. In order to have a broad main lobe, the waveforms Weil transform should have few zeros and an uncomplicated phase. To narrow the main lobe, we should add zeros and increase the complexity of the winding number structure.

With this in mind, we begin with a winding number matrix having a 1, 1, and -1 clustered around the center of the square, and no other nonzero values. S_1 will be the Gaussian product derived from this matrix. Its phase is essentially that of $\Theta(e^{-\pi t^2})$ and its modulus approximates $|\Theta(e^{-\pi t^2})|^3$. The third power serves to broaden the main lobe of the ambiguity surface. The waveform $s_1 = \Theta^{-1}(S_1)$ and a cross-section of its ambiguity surface are pictured in Figs. 22 and 23. The time and frequency cross-sections are identical so we include only one here.

In order to define S_2 we first consider the function S defined as

$$S = \prod_{i=1}^{s} G'_{\tau_i, f_i}, \tag{29}$$

where the winding numbers are the same as those of $\Theta(s)$ from section 3.1 (1, 7, 10, −4, −13), with the zeros being in a slightly different pattern. The waveform obtained from S via Θ^{-1} will certainly have a more narrow main lobe than s_1, however it will not in general be orthogonal to s_1. This is easily remedied. One may verify the following: S_1 is orthogonal to $S - \alpha$ where $\alpha = \alpha_1/\alpha_2$ with

$$\alpha_1 = \int_0^1 \int_0^1 S_1 \bar{S}\, dxdy \quad \text{and} \quad \alpha_2 = \int_0^1 \int_0^1 S_1\, dxdy. \tag{30}$$

In general care must be taken so that α is not large enough to destroy the zero pattern of S (α is small enough in this example). Our S_2 will then be $S - \alpha$ and we define s_2 as $\Theta^{-1}(S_2)$. As one might expect from its construction, s_2 looks essentially the same as s from section 3.1, shown in Fig. 1. Figures 24 and 25 depict the time and frequency cross-sections of the ambiguity surface of s_2.

We mention here as an aside that this construction may be extended to more than two levels of resolution. The next level in Weil space, S_3, would be constructed by multiplying S_2 by a doubly periodic function with enough zeros to narrow the main lobe a sufficient amount. That really is what we have done in this example. The winding number matrix for S_1 is an approximation to a submatrix of the winding number matrix for S_2 (or, equivalently, the matrix for S_1 is an actual submatrix of an approximation to the matrix for S_2).

Getting back to our example, we will assume that the scene is a distribution of point sources, and we present numerics for an example having two sources. Typically, given a waveform such as our $s(t)$, one might transmit a signal of the form

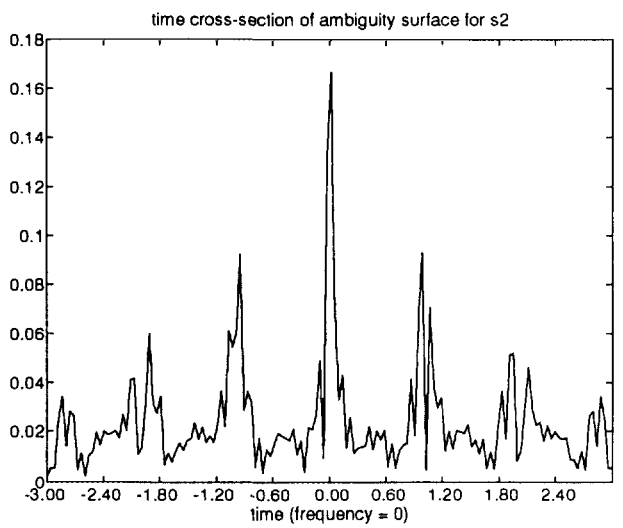

FIGURE 24

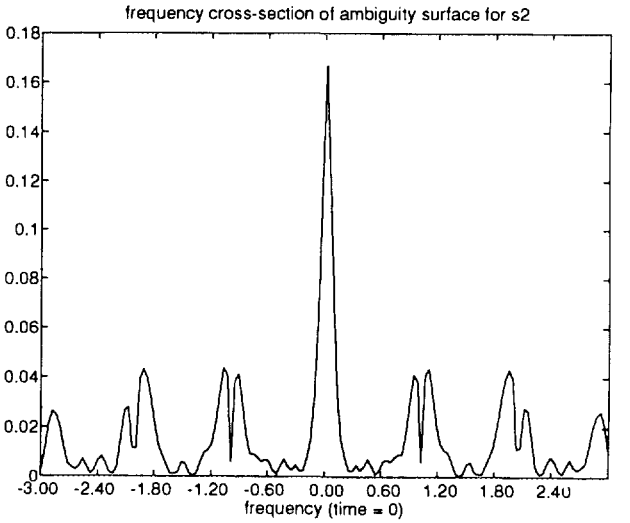

FIGURE 25

$$s(t)e^{2\pi i f_0 t} \tag{31}$$

where f_0 is a carrier frequency. Because the carrier term has no effect on the ambiguity calculations we are interested in, we will consider the transmitted signal to be just $s(t) = s_1 + s_2$. The return will then have the form

$$r(t) = s(t + \tau_1)e^{2\pi i\theta_1 t} + s(t + \tau_1)e^{2\pi i\theta_1 t} \tag{32}$$

where in this example we have set $\tau_1 = -1, \tau_2 = -.8, \theta_1 = .75$, and $\theta_2 = 1$. Note that we are using seconds and Hz as our units for τ and θ. These can be converted easily to actual range and Doppler values using $\tau = R/c$ and $\theta = f_0\nu/c$, where R is range, ν is speed, and c is the speed of light (see Blahut [9]). The separation of the two point sources is found to be approximately 50 miles in range of 18 miles per hour in speed if we assume a carrier frequency of 10^7 Hz and a bandwidth (from the Nyquist rate) of about 10^5 Hz. The relative location of the objects is the important issue as their locations within the time-frequency plane can be shifted (via translation and demodulation). Note also that what we are trying to exhibit is a computation-saving device for target recognition, not an advance in resolving power. The particular waveforms involved are used merely as an exercise in implementing the ideas of sec. 3.2.

The first processing of the return is computing the ambiguity surface $|A_{s,r}|$ on a grid in time-frequency space, with the computation being done on a coarse scale. The box size in time-frequency space of .4 by .4 is chosen based on the thickness of the main lobe for s_1. The values of the ambiguity surface in a neighborhood of its maximum value are displayed below, and Fig. 26 shows a gray-scale plot of the surface values. The peak values are sufficiently

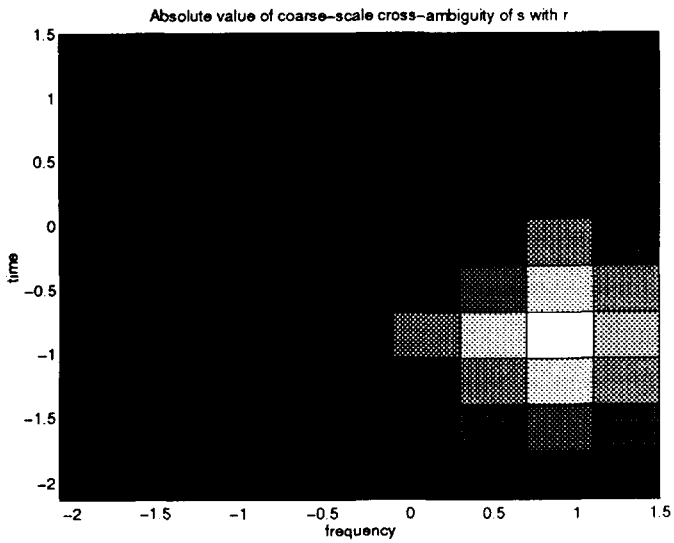

FIGURE 26

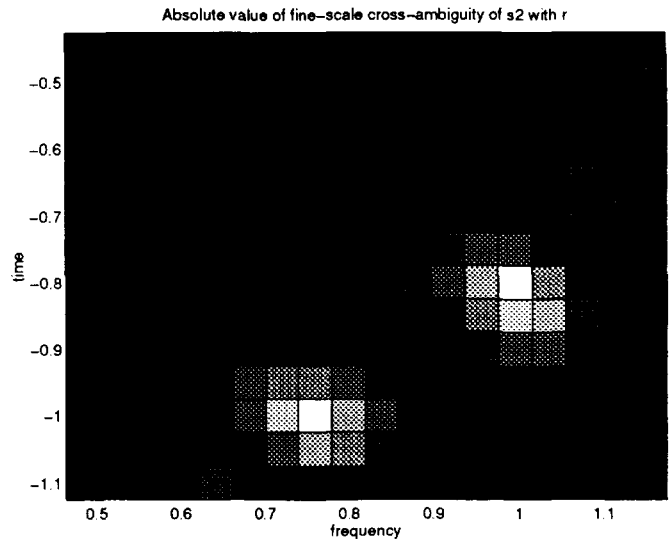

FIGURE 28

distinguished from the background to allow us to restrict to a small subset of the scene in doing a calculation at a finer scale. Note that the high values correspond to white and low values to black in the gray-scale plot, which also clearly tells us where to look for our target.

.0872	.2552	.4237	.2729	.0296
.3485	.5607	.7677	.5163	.2157
.5122	.7612	1.000	.7464	.4405
.1305	.4151	.7627	.5556	.2172
.1100	.1683	.5160	.3239	.0390

To obtain finer-scale information, we compute $|A_{s,r}|$ on a grid of bins in time-frequency space of size .05 by .05. But $s(t)$ itself is too coarse for this resolution, and in the area surrounding the two point sources we get a collection of ambiguity surface values that do not clearly distinguish a small part of the scene from the background. Too many of the values are very close to the maximum. The gray-scale plot in Fig. 27 shows this as a predominant glow around the center of the scene.

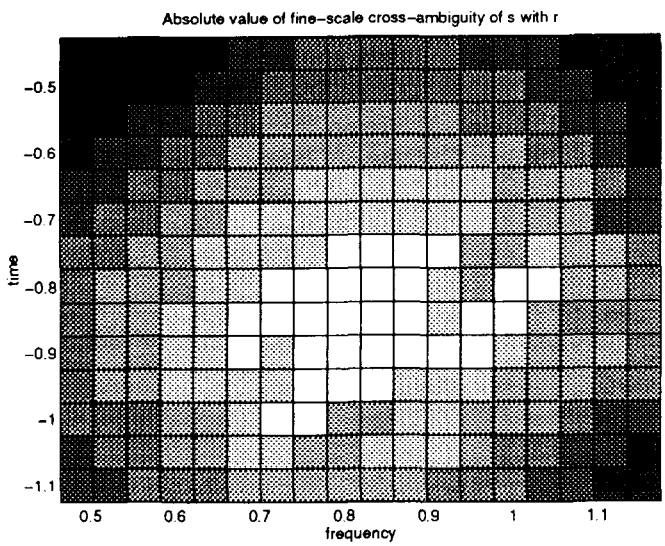

FIGURE 27

.9187	.8266	.8138	.8903	.8998
.9993	.9987	.8551	.8599	.8972
.8765	.9879	.9983	.9451	.9249
.9256	.9375	.9730	.9659	.9564
.9483	.9455	.9712	.9655	.9402

To resolve this dilemma, we merely compute the ambiguity surface $|A_{s_2,r}|$ on the .05 by .05 boxes in time-frequency space. The values from a neighborhood of the source corresponding to $\tau = -1$ and $\theta = .75$ are shown below, clearly delimiting a small part of time-frequency space in which to search for our target. Similar numbers occur in a neighborhood of the other source. Compare also the very black background of the corresponding gray-scale plot in Fig. 28 with that of Fig. 27.

.4733	.7308	.6198	.3656	.1944
.7825	1.000	.7378	.4276	.2313
.6022	.5872	.3887	.2146	.1227
.2403	.2340	.1107	.0022	.0586
.1514	.1402	.0479	.0762	.1714

Note that the ambiguity surface values here have been normalized to have maximum equal to one for purposes of

comparison. This example extends with success to more than two sources using the same computational scales.

4. CONCLUDING REMARKS

Each of the examples in Section 3, as well as the formation of pulse trains and their generalizations, may be considered as a technique for generating waveforms by modifying functions in H_1 through multiplication by doubly periodic functions. The general case is the generation of the waveform s defined by

$$s = \Theta^{-1}(Fp(x, y)), \tag{33}$$

where F is any H_1 function and $p(x, y)$ is any doubly periodic function. This operation is discussed in more mathematical terms in Auslander *et al.* [4]. Applications of this idea to problems in multi-access and spread-spectrum communications will be presented in Auslander and Warner [8]. Further investigation and expansion of this idea is warranted as evidenced by the interesting and potentially beneficial relationship of this idea to the problem of ambiguity surface generation and its relationship with communications.

REFERENCES

1. L. Auslander, Sliding windowed Fourier transforms and the Heisenberg group, "*Acoustic Signal Processing for Ocean Exploration*" (J. M. F. Moura and I. M. G. Lourtie, Eds.), 1993.
2. L. Auslander and F. Geshwind, Multi-target ambiguity functions, "*Acoustic Signal Processing for Ocean Exploration*" (J. M. F. Moura and I. M. G. Lourtie, Eds.), 1993.
3. L. Auslander and F. Geshwind, Approximate frames and the multitarget radar problem, *in* "*Proceedings of the 1992 NATO ASI on Wavelets and Their Applications,*" to appear.
4. L. Auslander, F. Geshwind, and F. Warner, "Weil Multipliers," to appear.
5. L. Auslander, F. Geshwind, M. Saadia-Otero, and F. Warner, The Weil transform and bandwidth, preprint.
6. L. Auslander and R. Tolimieri, "*Abelian Harmonic Analysis, Theta Functions and Function Algebras on a Nilmanifold,*" Lecture Notes in Mathematics 436, Springer-Verlag, New York, 1975.
7. L. Auslander and R. Tolimieri, Radar ambiguity functions and group theory, *SIAM J. Math. Anal.* **16** (1985), 577–601.
8. L. Auslander and F. Warner, Channel coding and waveform modification, in preparation.
9. R. E. Blahut, Theory of remote surveillance algorithms, *in* "*Radar and Sonar, Part I*" (R. E. Blahut *et al.*, Eds.), Springer-Verlag, 1991.
10. C. Cook and M. Bernfeld, "*Radar Signals: An Introduction to Theory and Applications,*" Academic Press, New York, 1967.
11. J. P. Costas, A study of a class of detection waveforms having nearly ideal range-Doppler ambiguity properties, *Proc. IEEE* **72** (1984), 996–1009.
12. I. Daubechies, The wavelet transform, time-frequency localization and signal analysis, *IEEE Trans. Inform. Theory* **36** (1990), 961–1005.
13. G. W. Deley, Waveform design, *in* "*Radar Handbook*" (M. I. Skolnik, Ed.), McGraw–Hill, New York, 1970.
14. G. B. Folland, "*Harmonic Analysis in Phase Space,*" Princeton Univ. Press, Princeton, 1989.
15. F. Geshwind, "The Weil transform and Ambiguity Functions," Thesis, CUNY, 1993.
16. S. Golomb and H. Taylor, Constructions and properties of Costas arrays, *Proc. IEEE* **72** (1984), 1143–1163.
17. J. R. Klauder, The design of radar signals having both high range resolution and high velocity resolution, *Bell System Tech. J.* **39** (1960), 809–819.
18. W. Miller, Jr., Topics in harmonic analysis with applications to radar and sonar, *in* "*Radar and Sonar, Part I*" (R. E. Blahut et al., Eds.), Springer-Verlag, 1991.
19. A. Rihaczek, Radar signal design for target resolution, *Proc. IEEE* **53** (1965), 116–128.
20. A. Weil, Sur certains groupes d'operatours unitaires, *Acta Math.* **111** (1964), 143–211.
21. P. M. Woodward, "*Probability and Information Theory, with Applications to Radar,*" Pergamon Press, Oxford, 1953.